Interactions of Hexafluoro-2-propanol with the Trp-Cage Peptide†

Chiradip Chatterjee and John T. Gerig*

Department of Chemistry and Biochemistry, University of California. Santa Barbara, California 93106

Received August 24, 2006; Revised Manuscript Received September 29, 2006

ABSTRACT: Fluoro alcohols present in aqueous solutions can alter the dominant conformations of peptides and proteins. The origins of these effects likely are related to the details of solute−fluoro alcohol interactions. Preferential interaction of the fluoro alcohol component of a fluoro alcohol−water mixture with peptide solutes has been demonstrated by several experimental approaches. In the present work, we have used $^{1}H\{^{19}F\}$ intermolecular NOE experiments to examine interactions of hexafluoro-2-propanol in a 30% fluoro alcohol−50 mM phosphate buffer solvent mixture with the "Trp-cage" peptide (NLY IQW LKD GGP SSG RPP PS). The results show that the peptide is selectively solvated by hexafluoro-2-propanol to the extent that the fluoro alcohol concentration near the peptide may be 3 to 4 times higher than the nominal concentration of fluoro alcohol in the bulk sample. The observed NOEs indicate that peptide−fluoro alcohol interactions persist for times of the order of 1 ns at 5 °C. As the sample temperature is increased, the lifetimes of fluoro alcohol interactions with several exposed side chains decrease to the extent that the peptide hydrogen−solvent fluorine interactions appear to become diffusive in nature, with interaction lifetimes of ∼0.03 ns. It is known that protein molecules can provide specific sites for binding small organic solvent molecules. Our work suggests that small peptides also have this ability and that the dynamics for such interactions can be site-specific.

Intermolecular interactions between solvent and solute are important to all chemical and biochemical phenomena, including protein folding, protein−protein interactions, and processes that take place at membrane surfaces. These solvent−solute interactions are difficult to characterize experimentally. Various NMR techniques are emerging as useful in this regard, with nuclear Overhauser effects being particularly important (*1*, *2*). Much of what is known about the interactions of water with biological molecules has been produced in these ways (*3*, *4*).

Small organic alcohols present in aqueous solution are known to alter the stability of dissolved peptides and proteins. Typically the presence of such materials favors the formation of helical conformations of small peptides but tends to induce unfolding of proteins. The effects on structure can be subtle, with switches between helical and extended structures being nonlinearly dependent on the amount of alcohol present (*5*−*7*). Characterization of partially folded states that form in alcohol−water solutions may be relevant to understanding the aggregation phenomena that are characteristic of protein misfolding diseases (*8*, *9*).

Fluorinated alcohols are more powerful in producing conformational effects than the corresponding nonfluorinated compounds (*10*). The reasons for the effectiveness of fluoro alcohols in altering the relative stability of conformations are not readily apparent but are likely related to the substantial hydrophobicity of the compounds and their ability to participate in hydrogen bonding. There is evidence for extensive preferential binding of the fluoro alcohol component of a water−fluoro alcohol solvent mixture to peptides and proteins, so that the local interactions between fluoro alcohol and water molecules are likely not those that are typical of the bulk solution (*11*, *12*).

A previous study in our laboratory examined intermolecular NOEs developed between the fluorines of hexafluoro-2-propanol (HFIP)[1] and the protons of the largely α-helical peptide melittin (*13*). Those results indicated that both water and HFIP molecules were tightly bound to the peptide in a bend region that separates two helical regions, while the remainder of the peptide exhibited NOEs consistent with preferential solvation of those regions by the HFIP component of the solvent in interactions that were short-lived and largely diffusive in nature. We wished to explore the hints from this work that the specificity and dynamics of fluoro alcohol interactions with peptides could be dependent on secondary structure. Dynamics depend on temperature, and we sought an experimental system that was small enough to be tractable in terms of the spectroscopy and had a conformation that included various secondary structure elements but was relatively stable as the sample temperature was changed. The 20-residue construct of Neidigh et al., commonly known as the "Trp-cage" peptide, met these requirements (*14*). This peptide folds in 4 μs to a compact globular structure that has helical and turn elements typical of larger proteins yet is small enough that molecular dynamics simulations of the system are practical (*15*, *16*). It has been shown that the peptide in 30% TFE remains substantially folded over the temperature range 0−40 °C (*14*).

† Support for this work was provided by a grant from the National Science Foundation (CHE-0408415).

* Corresponding author. Phone: 805-893-2113. Fax: 805-893-4120. E-mail: gerig@nmr.ucsb.edu.

[1] Abbreviations: HFIP, 1,1,1,3,3,3-hexfluoro-2-propanol-d_2; TFE, trifluoroethanol; TSP, 3-(trimethylsilyl)propionic acid-d_4 sodium salt.

10.1021/bi061750+ CCC: $33.50
Published on Web 11/14/2006

We report here that the Trp-cage peptide has a fold in 30% HFIP−water that is very similar to the reported conformation in 30% TFE and that the basic fold is retained up to 45 °C, albeit with the structure becoming more dynamic at higher temperatures. Intermolecular NOE experiments indicate that Trp-cage is selectively solvated by HFIP over the range 5−45 °C.

EXPERIMENTAL PROCEDURES

Materials

The Trp-cage peptide H_2N-NLY IQW LKD GGP SSG RPP PS-COOH was synthesized by Global Peptide Services (Fort Collins, CO) in >95% purity as assessed by HPLC and confirmed by mass spectrometry. 1,1,1,3,3,3-Hexafluoro-2-propanol-d_2 and undeuterated hexafluoro-2-propanol were obtained from Sigma-Aldrich. Deionized, distilled water was used for all sample preparations.

Methods

Sample Viscosity. Viscosities were determined with a Cannon (State College, PA) calibrated semimicroviscometer contained in a temperature control bath. Bath temperatures were determined by means of a calibrated thermometer. Pure water was used as a reference. Corrections for the density of the solutions were made using estimated densities obtained from molar volumes at various temperatures for HFIP−water solutions (*17*). The density estimated at 25 °C by this approach agreed with experimental data at this temperature (provided by Professor T. Yamaguchi). The apparent activation energy for change of viscosity with temperature for 30% HFIP−water was 24 kJ mol^{-1}, which is similar to the activation energies observed for changes of the viscosity of trifluoroethanol−water mixtures of a similar composition (*18*).

CD Spectroscopy. CD measurements were performed with an AVIV-202 spectropolarimeter equipped with a Peltier temperature control system using a 1 mm path length, demountable silica quartz cell. Samples were measured at wavelengths between 190 and 250 nm with a 1 nm step resolution and an integration time of 3 s. Spectra were an average of 16 scans and were baseline corrected. Sample temperatures were determined (±1 °C) with a calibrated thermocouple (Fisher Scientific). Each experiment was equilibrated at a temperature for 30 min before the spectrum was recorded. The peptide concentration was determined by UV spectroscopy using $\epsilon_{278} = 6760$ cm^2 $mmol^{-1}$.

NMR Spectroscopy. NMR spectra were collected using a Varian INOVA instrument operating at a proton frequency of 500 MHz. A Nalorac H/F probe equipped with a *z*-axis gradient coil was used. Sample temperatures were determined using a standard sample of methanol (Wilmad) and are believed to have been constant to better than ±0.1 °C during the course of an experiment and accurate to better than ±0.5 °C. The probe was detuned as necessary to avoid the effects of radiation damping.

Samples for NMR experiments were ~5 mM in peptide and contained 50 mM phosphate buffer and 10% D_2O. Apparent sample pH was determined by a Model IQ150 pH meter (IQ Instruments, San Diego, CA) equipped with a 4 mm o.d. stainless steel electrode. The reported pH was not corrected for the presence of fluoro alcohol or for isotopic composition.

Self-diffusion coefficients were determined by bipolar pulse pair−longitudinal eddy current delay (*19*), double multiple spin echo (*20*) and bipolar double stimulated echo (*21*) pulsed field gradient methods. The latter methods suppress the effects of convection within the sample; these effects were most likely to be prevalent at temperatures above or below room temperature. Gradient values and timing parameters for a pulse sequence which led to a 2−3 orders of magnitude change of the signals of interest were used. Samples were allowed to equilibrate in the probe at the regulated temperature at least 3 h before diffusion measurements were attempted. Consideration of the reproducibility of the diffusion coefficients and their sensitivity to the parameters used in the experiments suggests that the values quoted below are reliable to at least ±15%. Given the insensitivity of the conclusions reported below to the accuracy of these diffusion coefficients, it did not seem profitable to strive for greater accuracy.

Assignment of the proton signals of Trp-cage was accomplished by consideration of TOCSY and NOESY spectra that were collected using pulse sequences based on those of Fulton and Ni (*22*). TOCSY mixing times were typically 70 ms; NOESY mixing time ranged from 50 to 200 ms. Signal assignments at each temperature are reported in the Supporting Information.

$^1H\{^{19}F\}$ and $^1H\{^1H\}$ intermolecular cross-relaxation parameters (σ_{HX}) were determined by the procedures previously described (*13*, *23*, *24*). Observed NOEs were determined for a range of mixing times (t_{mix}) and fit to the empirical function $At_{mix} + Bt_{mix}^2$, with the coefficient A ($\equiv\sigma_{HX}$) being taken as the initial slope of the data. (Since intramolecular proton−proton dipolar interactions are present and other spins of the peptide may be interacting with solvent molecules, the development of the intermolecular NOEs will be described by a polyexponential function. The equation we use represents the leading terms in the function that describes development of the NOE when the mixing times are short.) All data were corrected for the extent of inversion of spin X. The experiments for intermolecular NOE determinations were extensively signal-averaged to minimize the effects of instrumental instabilities.

Molecular modeling and visualization were done with SYBYL (Tripos), PYmol (DeLano Scientific LLC), and MOLMOL (*25*).

Solvent molecules were represented by spheres for calculations of intermolecular solvent−peptide cross-relaxation parameters. The apparent radii of solvent molecules used in this work were estimated by constructing a model in SYBYL using standard bond lengths and angles. After the conformational energy was minimized, a van der Waals surface for the model was calculated using the Connolly method (*26*). The radius of the sphere "rolled" over the surface of the model in these calculations was 1.2 Å, corresponding to the van der Waals radius of a covalent hydrogen (*27*). Distances from the surface defined by the probing spheres to the center of the molecule were calculated and averaged. It was estimated by this approach that the radii of HFIP and water are 2.79 and 1.66 Å, respectively. The radius for HFIP is similar to the value (3.14 Å) estimated by considering the neat liquid to be a collection of spheres arranged in cubic

Table 1: Structural Statistics for Trp-Cage in 30% HFIP−50 mM Phosphate Buffer

	5 °C	25 °C	45 °C
no. of cross-peaks assigned	331	289	216
no. of unassigned cross-peaks	9	5	5
no. of NOE constraints used in structure analysis	158	112	78
mean ensemble rmsd (Å)			
backbone atoms	0.60 ± 0.23	1.41 ± 0.50	2.00 ± 0.60
heavy atoms	1.32 ± 0.29	1.98 ± 0.41	2.60 ± 0.56
Ramachandran statistics (%)			
residues in most favored region	81.8	81.8	73.7
residues in additionally allowed regions	18.2	18.2	27.3

closest packed lattice (*28*). The same approach was used to estimate the radii of spheres representing Trp-cage and TSP, which were 8.9 and 3.5 Å, respectively.

Expected cross-relaxation rates (σ_{HX}) due to intermolecular dipolar interactions were estimated as previously described (*24*). The method takes into account the shape of a solute molecule (represented by its Connolly surface) but approximates solvent molecules as spheres. It has been shown that, for any reasonable set of conditions, the interacting spins of a solvent molecule behave as if they are positioned at the center of the representative sphere (*29*). Experimental self-diffusion coefficients were used in the calculations.

NOESY data were analyzed to provide proton−proton distance constraints for structure determinations using the program SPARKY (*30*). Detail regarding the observed NOEs is given in the Supporting Information. A small number of unassignable NOE cross-peaks were present in the NOESY data at all temperatures. These presumably arise from minor conformations of the four proline residues present in Trp-cage and were ignored. The program DYANA was used to find conformations consistent with the assigned $^1H\{^1H\}$ NOEs (*31*, *32*). The ten best structures defined by DYANA were then relaxed in the AMBER 4.1 force field with the same distance constraints using SYBYL (Tripos). The energy penalty function for violation of a NOE constraint was $E_{NOE} = k(d - d_0)^2$, where d_0 is the upper or lower bound for a particular H−H distance, d is this distance in a particular conformation, and the constant $k = 30$ kcal mol^{-1} Å^{-2} (*33*). The experimental dielectric constant of 30% HFIP (60) was used in the electrostatic part of the force field (*34*).

RESULTS

Structure of Trp-Cage in 30% HFIP/Water. The structures of Trp-cage under the conditions of our experiments were determined by standard methods involving the generation of interproton distance constraints from observed intramolecular $^1H\{^1H\}$ NOEs. Proton spectra of Trp-cage in HFIP−buffer solutions were similar to that reported for the peptide in trifluoroethanol−buffer (*14*), and assignment of the spectra obtained at various temperatures in 30% HFIP−water was appreciably aided by the assignments in TFE−water provided by Neidigh et al. Fewer NOEs were observed as the sample temperature was increased from 5 to 45 °C (Table 1), presumably as a result of increased rates of unfolding and local conformational transitions. Consequently, the bundle of best-fit structures calculated at the higher temperature showed a larger rmsd of the atom positions than was the case at the lowest temperature.

Figure 1A compares the mean structure of Trp-cage in 30% HFIP at 5 °C to the mean structure in 30% TFE at 9 °C previously reported by Neidigh et al. (*14*). The rmsd of the backbone atoms of the two structures is 0.99 Å while the rmsd of all heavy atoms is 1.73 Å. It is clear that, within the reliability of the methods used, the structure in HFIP is essentially the same as that in TFE.

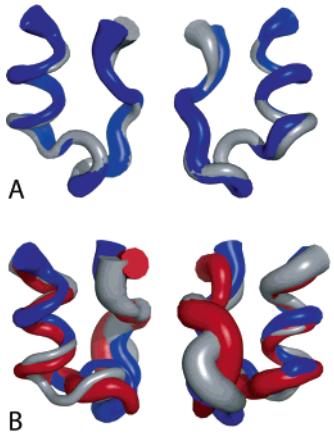

FIGURE 1: (A) Comparison of the conformation of Trp-cage in 30% HFIP−50 mM phosphate buffer (blue) at 5 °C found in this work with that in 30% TFE−15 mM phosphate buffer at 9 °C (gray) (*14*). (B) Comparison of the structures of Trp-cage in 30% HFIP found at 5 °C (blue), 25 °C (gray), and 45 °C (red). The second view given for each system is obtained by rotating the first view 180° around the vertical axis. In each drawing, the diameter of the tube is proportional to the rmsd of the backbone atoms in a structure bundle of the 10 lowest energy conformations that are consistent with NMR-derived distance constraints.

Figure 1B compares the structures in HFIP at three temperatures. Considering root-mean-square deviations, the structures of Trp-cage in HFIP found at 25 and 45 °C are not as well-defined as is the conformation of the peptide at 5 °C. It is seen that, nonetheless, the overall fold of the peptide is virtually the same at all temperatures.

The chemical shifts of Trp6 $H_{\epsilon 3}$, Gly11 $H_{\alpha 2}$ and $H_{\alpha 3}$, Pro18 H_α, $H_{\beta 2}$, and $H_{\beta 3}$, and Pro19 $H_{\delta 2}$ and $H_{\delta 3}$ are strongly influenced by the magnetic anisotropies of the aromatic rings of the Tyr3 and Trp6 residues. These shifts are thus sensitive to conformation and have been used as indicators of the folding of the peptide (*14*, *35*). We note that the shifts of these protons in HFIP are nearly the same as the (unusual) shifts observed when the solvent is TFE and that the shifts change only slightly with temperature. We conclude that the mean tertiary structure of Trp-cage in 30% HFIP is essentially independent of temperature over the range 5−45 °C.

Temperature coefficients of the peptide N−H chemical shift were calculated (Table 2). In water, the peptide proton chemical shifts of unstructured peptides typically have temperature coefficents in the −10 to −6 ppb/K (*36*). This

Table 2: Amide Proton Chemical Shift Temperature Coefficients

residue	$\Delta\delta/\Delta$T (ppb/K)	residue	$\Delta\delta/\Delta$T (ppb/K)
Leu2	−2.1	Gly10	−2.0
Tyr3	−1.6	Gly11	−3.5
Ile4	−4.5[a]	Ser13	−0.85
Gln5	−6.4[a]	Ser14	−2.0
Trp6	0.60	Gly15	−0.85
Leu7	−1.2	Arg16	−2.1
Lys8	−5.5	Ser20	−0.95
Asp9	−2.3		

[a] Shifts of these protons were nonlinear over the temperature range studied. The value given was the approximate slope in the range 25−45 °C.

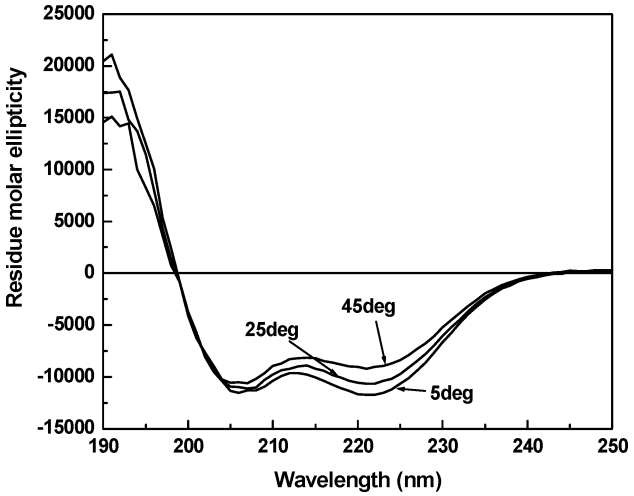

FIGURE 2: CD spectra of 80 μM Trp-cage in 30% HFIP−50 mM phosphate buffer at pH 7 at various temperatures.

appears also to be the case for solvents containing trifluoroethanol (*37*). While there can be influences of sequence and solvent composition, temperature coefficients that are appreciably more positive than this range have been taken to indicate that a peptide N−H is involved in intramolecular hydrogen bonding. The values of $\Delta\delta/\Delta T$ observed in the present work are generally consistent with intramolecular hydrogen bonding in the α-helical region from residues 2 to 10 and the near-α-helical structure from residues 11 to 15 structures shown in Figure 1.

Deviations of observed α-proton chemical shifts from the corresponding random coil values, corrected for sequence dependence according to the description of Schwarzinger et al. (*38*), were analyzed and are also indicative of a helical conformation from residues 2 to 15 (*39*). A plot of these data is given in the Supporting Information.

Circular Dichroism Measurements. CD spectra for Trp-cage in 30% HFIP−buffer recorded over the temperature range used in the present work are shown in Figure 2. Data from 198 to 250 nm were analyzed using the program CDSSTR (*40*). The analyses indicated that 65−70% of Trp-cage is present in α-helical, distorted α-helical, or turn conformations, a result reasonably consistent with the structures shown in Figure 1.

It should be noted that the CD spectra were recorded at peptide concentrations lower than those used for the NMR experiments.

Interactions of HFIP with Trp-Cage. Interactions of the HFIP component of the 30% HFIP−50 mM phosphate buffer solvent with the peptide were explored by determination of

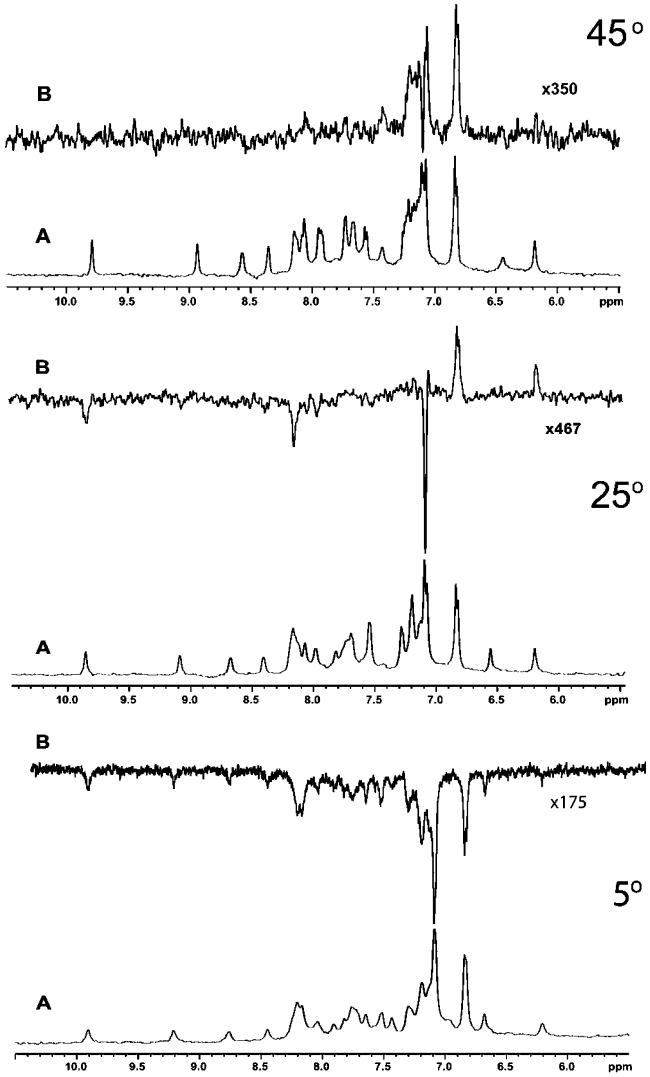

FIGURE 3: Proton−fluorine intermolecular NOE spectra at 500 MHz of Trp-cage in 30% HFIP−50 mM phosphate buffer at various temperatures. The concentration of the peptide was 5 mM, and the sample pH was 7.0. Spectrum A in each set is the observed 1D proton spectrum; spectrum B is the proton−fluorine NOE spectrum at a mixing time of 600 ms. Horizontal and vertical scales for the sets of spectra are slightly different. Positive signals in the NOE spectrum correspond to positive values of σ_{HF}^{NOE}. At all temperatures the intermolecular NOE on the TSP reference signal was positive (Figure 4).

the intermolecular NOEs developed between the solvent fluorine atoms and hydrogens of the peptide (Figures 3 and 4). As will be discussed below, the $^1H\{^{19}F\}$ NOEs are expected to be positive on the basis of the relative diffusion of the peptide and fluoro alcohol. However, the only positive intermolecular NOE observed at 5 °C is the one arising from interactions of the solvent with the TSP reference compound (Figure 4). The other positive NOE observed in this spectrum is the result of intramolecular hydrogen−fluorine interactions in molecules of HFIP where a proton remains at position 2 in the alcohol due to incomplete deuteration. Not all protons of Trp-cage show detectable solvent Overhauser effects at 5 °C, but the NOEs to peptide hydrogens that are observed are all negative (Figure 3).

Increasing the sample temperature to 25 °C leads to spectra in which both positive and negative solute proton−solvent fluorine NOEs are observed (Figure 3). At 45 °C, most NOEs

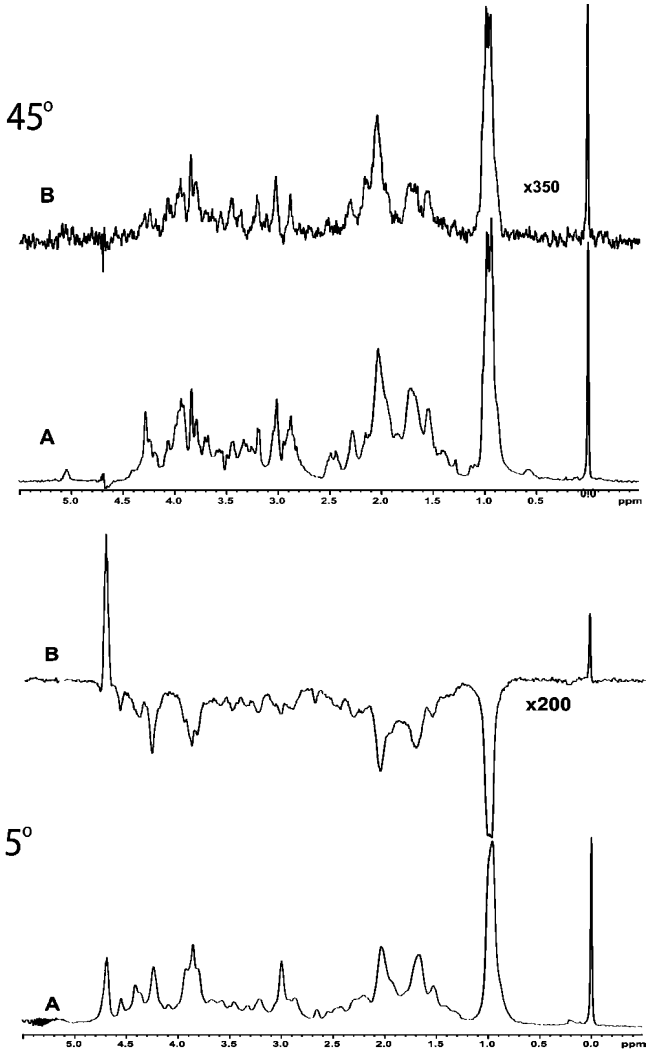

FIGURE 4: Upfield portions of proton−fluorine intermolecular NOE spectra at 500 MHz of Trp-cage in 30% HFIP−50 mM phosphate buffer. Conditions for each experiment were the same as those used to collect the data shown in Figure 3. Spectrum A in each set is the observed 1D proton spectrum; spectrum B is the proton−fluorine NOE spectrum at a mixing time of 600 ms. Horizontal and vertical scales for the two sets of spectra are slightly different. Spectra of this region at 25 °C are given in the Supporting Information.

are positive although in the low-field part of the spectrum many NOEs disappear and at least one NOE (at 7.2 ppm) remains negative (Figures 3 and 4).

The observed peptide proton−solvent fluorine NOEs determined as a function of mixing time can be summarized by means of the cross-relaxation parameter σ_{HF}. These parameters were estimated for signals in the proton spectra of Trp-cage that could be reasonably confidently assigned; these data are collected in Table 3. Cross-relaxation data for the TSP reference signal are presented in Table 6.

Rotational and Translational Diffusion. Interpretation of the cross-relaxation rates (σ_{HF}^{NOE}) reported here requires estimates of the translational diffusion coefficients of the solution components. These were determined by NMR experiments and are recorded in Table 4.

Diffusion measurements by NMR methods are subject to convection effects when the sample temperature is not near room temperature, particularly at temperatures above room temperature (*41*). Pulse sequences to minimize these effects

Table 3: Intermolecular Proton−Fluorine Cross-Relaxation Rates for Trp-Cage[a]

	σ_{HF}^{NOE} ($s^{-1} \times 10^3$)					
proton	obs at 5 °C	calc at 5 °C	obs at 25 °C	calc at 25 °C	obs at 45 °C	calc at 45 °C
Asn1 $H_{\delta 22}$	∼0	5.8	2.3	4.4	4.5	4.0
Leu2 $Q_{\delta 1}$, Ile4 $Q_{\delta 2}$, Leu7 $Q_{\delta 2}$, Leu2 $Q_{\delta 2}$[b]	−9.5 to −7.0	1.7 to 6.6	2.4 to 3.8	1.7 to 5.7	7.8 to 8.2	1.4 to 3.5
Leu2 H_N		0.0	∼0	0.9	∼0[d]	1.4
Leu2 $H_{\beta 2}$	−9.9[d]	0.8		2.8		1.2
Tyr3 H_N	−18[d]	−1.2		0.5	∼0	0.5
Tyr3 Q_δ	−17[d]	0.7	+[c]	3.0	5[d]	1.6
Tyr3 Q_ϵ	−11	2.9	2.1	4.4	14	3.2
Ile4 H_N	−18[d]	−1.2	∼0	0.9	∼0	0.5
Gln5 H_N		−1.2		−0.1	∼0[c]	0.4
Gln5 Q_β		2.3	−11	0.6		1.1
Gln5 Q_γ		1.5	−1.2	3.8		2.4
Gln5 $H_{\epsilon 21}$		4.3	∼0	6.7	2	2.9
Gln5 $H_{\epsilon 22}$	−23	0.6	∼0	5.6	∼0	2.1
Trp6 H_N	−18[d]	−0.9	−2[c]	−0.1	∼0	0.2
Trp6 $H_{\delta 1}$	−17[d]	0.5	−10[d]	2.1	5[d]	0.4
Trp6 $H_{\epsilon 1}$	−29	−1.0	−7.8	0.7	∼0	0.7
Trp6 $H_{\epsilon 3}$		−1.1	∼0[c]	−0.1	∼0	0.6
Trp6 $H_{\eta 2}$		2.7		3.0	7.4	2.7
Trp6 $H_{\zeta 3}$	−13	1.9		2.5		2.3
Leu7 H_N	−13	−1.4	−[b]	−0.3	∼0	0.4
Leu7 H_γ	−5.6[d]	0.5		0.2		3.0
Lys8 H_N	−[c]	−1.1	−[b]	0.2	∼0	0.7
Lys8 H_α		2.4	1.7	3.6		2.8
Lys8 Q_δ	−9.9[d]	2.6		3.5		2.5
Asp9 H_N	−7	−1.1	−14.	0.6	∼0[d]	0.7
Gly10 H_N		−1.3	∼0	0.2	∼0[d]	2.4
Gly11 H_N	−[c]	−1.3	∼0	−0.05	∼0	0.9
Pro12 H_α	−11	2.2		1.3		1.5
Pro12 $H_{\beta 3}$		4.7	−5.6	4.9	3	3.2
Pro12 $H_{\gamma 2}$		4.5		4.8	7[d]	2.6
Ser13 H_N		−0.6	∼0	1.2		1.1
Ser13 H_α		3.4	−3.2	4.5	∼0[d]	1.1
Ser14 H_α	−15[d]	3.1	−2[d]	4.5	∼0	1.2
Gly15 H_N	−7	−1.1	∼0	0.6	∼0[d]	2.9
Arg16 H_N	−18[d]	−0.1	−2[d]	2.9	2	1.2
Arg16 H_α	∼0	1.2		2.9	∼0	2.4
Arg16 $H_{\beta 3}$		0.9	−7.9	3.0		1.4
Arg16 $H_{\delta 2}$		1.9	−9	6.8		1.4
Arg16 H_ϵ		−1.0	−10[c]	7.5	5[d]	3.9
Pro17 $H_{\beta 3}$		5.0		4.6	3	0.9
Pro17 Q_γ	−5.6[d]	4.5		4.1		4.0
Pro18 $H_{\beta 2}$		4.0	3.8	−0.06		0.9
Pro19 H_α	−15[d]	3.1	3.2	2.0		2.8
Pro19 $H_{\beta 2}$	−9.9[d]	2.5		4.6	7[d]	3.3
Ser20 H_α		1.4	0.2	4.5		2.9
Ser20 $H_{\beta 3}$	−5.8	5.3		6.7	3.8	4.1

[a] Calculated values of σ_{HF}^{NOE} were obtained using the experimental diffusion coefficients at each temperature and molecular shapes as described in Experimental Procedures. Diastereotopic or methyl protons that could not be distinguished on the basis of their chemical shifts are indicated by Q. [b] Range of values given for the overlapped signals of the peptide methyl groups. [c] NOE barely detectable but probably has the sign indicated. [d] Overlapped with another signal.

were used. In order to check on the magnitude of the observed translational diffusion coefficients, the microviscosity approach of Gierer and Wirtz was used to estimate these (*42*). The predicted diffusion coefficients agreed with experimental results to within a factor of 2.

Rotational correlation times (τ_R) for Trp-cage were estimated from the Debye equation $\tau_R = 4\pi\eta r^3/(3kT)$, where η is the solvent viscosity and r is the radius of the sphere representing the solute (*43*). Alternatively, τ_R was estimated

Table 4: Experimental Translational Diffusion Coefficients ($\times 10^6$ cm^2 s^{-1})[a]

	5 °C	25 °C	45 °C
Trp-cage	0.45	0.82	5.4
water	5.7	12	17
HFIP	2.3	4.5	10
TSP	1.1	2.4	8.4

[a] The sample contained 5 mM Trp-cage, 0.05 M phosphate buffer at pH 7.0, and 30% HFIP. Data at 5 °C were collected using the DSTE pulse sequence. Data at 45 °C were collected using the DMSE pulse sequence.

from $\tau_R \approx (2r^2)/(9D_{tran})$, where D_{tran} is the experimental translational diffusion coefficient (*44*). The two approaches agreed to within 25%. For the calculations described below, the values of τ_R at 5, 25, and 45 °C used in calculations were 3.1, 1.2, and 0.7 ns, respectively.

Analysis of Peptide Proton−Solvent Fluorine Cross-Relaxation. Intermolecular nuclear Overhauser effects arise from dipolar interactions between spins of the solute and spins of the solvent molecules. A typical theoretical description of these interactions when solute and solvent molecules randomly encounter one another has been given by Ayant et al. Their treatment leads to the equation (*45*):

$$\sigma_{HF}^{NOE} = \frac{1}{10}\gamma_H^2\gamma_F^2h^2\frac{N_F}{\pi Db}[-J_2(\omega_H - \omega_F) + 6J_2(\omega_H + \omega_F)] \quad (1)$$

where γ_H and γ_F are the gyromagnetic ratios, h is Planck's constant, N_F is the number of solvent fluorine spins per milliliter, D is the sum of the diffusion coefficients for the solute and solvent species, b is the distance of closest approach of solute and solvent spins, and J is a spectral density function given by

$$J_2(\omega) = [3\omega\tau + (15/\sqrt{2})(\omega\tau)^{1/2} + 12]/[(\omega\tau)^3 + (4/\sqrt{2})(\omega\tau)^{5/2} + 16(\omega\tau)^2 + (27/\sqrt{2})(\omega\tau)^{3/2} + 81\omega\tau + (81/\sqrt{2})(\omega\tau)^{1/2} + 81] \quad (2)$$

with the parameter τ equal to b^2/D. Equation 1 indicates the important considerations that define an experimental value of σ_{HF}^{NOE}, including the concentration of solvent (fluorine) spins, the mutual diffusion of solute and solvent ($D = D_{solute} + D_{solvent}$), the minimum distance for solute spin−solvent spin interaction, and the spectrometer frequency.

Equation 1 has been derived with the assumption that the proton observed is located within a spherical structure of radius r_H and the solvent fluorine is within a sphere of radius r_F so that $b = r_H + r_F$. It has been shown that it is a good approximation to regard solvent spins as being localized at the center of a representative sphere (*29*). However, the assumption that the solute is a sphere leads to overestimated values of σ_{HF}^{NOE} since not all approaches of solvent molecules to a large solute can involve the same interaction distance. We have developed a numerical method that recognizes the shape of the solute molecule. Values of σ_{HF}^{NOE} estimated by this method generally agree well with experimental observations (*13*, *23*, *24*).

Several situations may arise when interpreting experimental values of σ_{HF}^{NOE}. (1) These values of σ_{HF}^{NOE} may be close to those predicted by using treatments such as eq 1 and experimental values of the diffusion coefficients, the bulk concentration of solvent spins, and reasonable estimates of molecular sizes and shapes. An inference that can be drawn in this instance is that solvent and solute molecules encounter each other primarily through random diffusion and that specific solvent−solute interactions are absent. (2) When a predicted σ_{HF}^{NOE} does not agree with experiment, it may be the case that the concentration of solvent spins near the solute is different from the bulk concentration. There is evidence for such "solvent sorting" in mixed organic−aqueous solutions (*46*−*48*). (3) Disagreement of predicted values of σ_{HF}^{NOE} with experiment may also indicate that the diffusion of solvent and solute molecules when they are close to one other is different from their diffusive behavior in the bulk of the solution where solvent−solvent interactions will be dominant. Theoretical descriptions of this situation have been presented (*49*, *50*). Although it is known that a layer of water molecules near proteins has translational and rotational dynamics that are different from the dynamics characteristic of bulk water (*4*, *51*), there have been few experimental demonstrations of the phenomenon, particularly in mixed solvent systems (*49*). (4) It may be the case that the model and assumptions such as isotropic pair correlation functions and force-free diffusion used in treatments such as eq 1 do not correspond to the situation under study, resulting in disagreements between theoretical predictions and experimental observations.

Calculations of σ_{HF}^{NOE} cross-relaxation parameters expected for interactions of HFIP with Trp-cage if these interactions involve random encounters of solvent and solute molecules (case 1) were done using the experimental diffusion coefficients and our procedure for taking into account the shape of the peptide. The results of these calculations are given in Table 3. In most cases, the predicted cross-relaxation rate for interaction of HFIP with a peptide hydrogen is positive. It is striking that many of the experimental σ_{HF}^{NOE} cross-relaxation parameters obtained in this work are negative, particularly at the lower sample temperatures. When negative values of σ_{HF}^{NOE} were predicted, they were generally an order of magnitude different from the experimental values.

Models involving altered diffusion of solvent molecules near the peptide were explored to address the disagreements between observed and predicted cross-relaxation rates. Cases considered included those in which layers of solvent one or two molecules thick adjacent to the peptide had diffusion coefficients that ranged from half to twice the experimental value for the bulk solvent. In no instance were predicted cross-relaxation parameters obtained that were very much different from the calculated values given in Table 3.

A process fundamentally different from random solvent−solute collisions must be operating in the HFIP−Trp-cage system to produce the observed σ_{HF}^{NOE} cross-relaxation parameters, particularly at 5 °C. We propose that these σ_{HF}^{NOE} not only include the effects of random interactions of the fluorinated solvent molecules with the protons of Trp-cage but also contain a significant contribution from the formation of relatively long-lived complexes between the fluoro alcohol and the peptide. If such complexes persist long enough, the dipolar interactions between Trp-cage hydrogens and HFIP

fluorines become, in effect, intramolecular interactions so that the motions modulating the interactions are those associated with the rotational diffusion of the complex. Halle has shown that the contribution of such long-lived associations of solute and solvent molecules leads to an additional term in the expression for σ_{HF}^{NOE} given by eq 3 (*49*).

$$\sigma_{HFcomplex}^{NOE} = \frac{1}{10}\gamma_H{}^2\gamma_F{}^2\hbar^2[-J'_2(\omega_H - \omega_F) + 6J'_2(\omega_H + \omega_F)] \quad (3)$$

The spectral density function J_2' is defined as

$$J_2'(\omega) = \sum_{k=1}^{N} \frac{n_k}{r_k{}^6}\left(\frac{\tau_{C,k}}{1 + \omega^2\tau_{C,k}{}^2}\right) \quad (4)$$

The summation in eq 4 is taken over N classes of solvent molecules, each class containing n_k solvent spins at a distance r_k from the solute proton of interest. Interaction(s) with the solute proton is (are) characterized by the correlation time $\tau_{C,k}$, defined by $1/\tau_{C,k} = 1/\tau_R + 1/\tau_{M,k}$, where τ_R is the rotational correlation time of the complex, taken here to be the same as the rotational correlation time of the peptide, and $\tau_{M,k}$ is the mean residence time of the spins of the class in the complex.

Consideration of the data in Table 3 indicates that at 5 °C the protons of Trp-cage exhibit values of σ_{HF}^{NOE} that are about 15×10^{-3} s^{-1} more negative than expected on the basis of the random collisions of solute and solvent model. At 25 °C, the observed σ_{HF}^{NOE} are both positive and negative, but in many instances it appears that the observed cross-relaxation terms are about 8×10^{-3} s^{-1} more negative than expected. At 45 °C, many σ_{HF}^{NOE} appear to be near zero, which could be the case if there is a $(1-2) \times 10^{-3}$ s^{-1} negative contribution to σ_{HF}^{NOE} that counters the positive contribution that arises from the random interactions of peptide and fluoro alcohol molecules. It can be calculated using eq 3 that a single HFIP molecule (6 equiv of fluorine, $n_k = 6$) with a mean residence time $\tau_{M,k} \approx 10^{-9}$ s at a distance of 4.65 Å from a solute proton would produce contributions to σ_{HF}^{NOE} of -16×10^{-3} s^{-1}, -8×10^{-3} s^{-1}, and -2×10^{-3} s^{-1} at 5, 25, and 45 °C, respectively. (The contribution to σ_{HF}^{NOE} varies due to the variation of the rotational correlation time of Trp-cage with temperature.) These calculations thus suggest that the discrepancies between observed and calculated cross-relaxation rates can be explained by postulating that a HFIP solvent molecule within near van der Waals contact of a Trp-cage hydrogen participates in an interaction that persists for of the order of 1 ns. There are, of course, many ways to achieve the same calculated contributions to σ_{HF}^{NOE} since the number of classes of interacting fluoro alcohol molecules, the number of fluorines in each class, and the mean lifetimes within a class used in applying eq 3 can be adjusted over a wide range. Our calculations merely indicate that the formation of relatively long-lived complexes between Trp-cage and the HFIP molecules of the solvent system is compatible with the observed cross-relaxation parameters.

As temperature increases, the proton−fluorine cross-relaxation rates for the side chain hydrogens of Leu2, Tyr3, Ile4, Trp6, Leu7, Pro12, Pro17, and Pro19 increase. At 45 °C, σ_{HF}^{NOE} values for these hydrogens are 3−4 times *larger* than expected on the basis of the experimental diffusion coefficients of Trp-cage and HFIP. Similar observations have been made in other systems involving peptides dissolved in mixed fluoro alcohol−water solutions (*13*, *47*) and have been interpreted to mean that the local concentration of fluoro alcohol near a peptide is higher than the bulk concentration of the fluoro alcohol. We note that the local concentration of fluoro alcohol cannot exceed that of the pure alcohol, so values of σ_{HF}^{NOE} more that 3.3 times the predicted value, such as that for Tyr3 Q_ϵ, cannot be explained entirely in this way. Calculations with eq 3 indicate that larger than expected values of σ_{HF}^{NOE} are also consistent with the presence of long-lived peptide−fluoro alcohol complexes in which the lifetime of the complex has been shortened to ∼0.4 ns.

Table 5: Methyl Proton−Water Proton Cross-Relaxation Rates[a]

	$\sigma_{HH}^{NOE} \times 10^3$ s^{-1}	
sample temp (°C)	obs	calc
5	−51	38
25	−10	24
45	7.6	15

[a] The sample contained 5 mM Trp-cage, 0.05 M phosphate buffer at pH 7.0, and 30% HFIP. Data are for the tallest peak within the collection of signals arising from the methyl groups of Leu2, Ile4, and Leu7.

If the local concentration of fluoro alcohol is larger than the bulk concentration, then the local concentration of water molecules presumably is lower that the bulk concentration of water. Thus, one would anticipate that cross-relaxation rates between Trp-cage protons and the protons of water molecules would be smaller than predicted on the basis of the random encounter model. Interpretation of water−peptide NOEs is complicated by processes that exchange water protons for protons of the peptide (*3*, *52*), and the contribution of exchange processes to experimental NOEs to peptide protons and protons that have dipolar interactions with peptide protons must be taken into consideration. We determined cross-relaxation parameters for water proton−peptide methyl proton interactions in the hope that exchange effects would be minimal for these spins which are presumably distant from the N−H sites of exchange. Table 5 presents a comparison of experimental values for these cross-relaxation rates to cross-relaxation values calculated using the assumption of random encounters of water and peptide molecules controlled by the experimental diffusion coefficients. The negative cross-relaxation rates (σ_{HH}^{NOE}) at 5 and 25 °C are consistent with the presence of interactions of the peptide methyl hydrogens with water molecules that are strongly bound to the peptide, similar to what appears to be the case for the interactions of HFIP molecules at these temperatures. At 45 °C, HFIP interactions with peptide methyl groups seem to involve only diffusive encounters. Provided there are no negative contributions to σ_{HH}^{NOE} from tightly bound water molecules at 45 °C, the smaller than expected experimental σ_{HH}^{NOE} is consistent with a reduction of the concentration of water in the vicinity of the Trp-cage surface.

Solvent−Solute Cross-Relaxation with the Reference Compound. The hydrogens of the TSP reference compound

Table 6: Intermolecular Cross-Relaxation Rates for the TSP Reference Signal

	$\sigma_{HF}^{NOE} \times 10^3$ s^{-1}		$\sigma_{HH}^{NOE} \times 10^3$ s^{-1}	
sample temp (°C)	obs	calc	obs	calc
5	6.8	4.9	11	36
25	8.2	4.8	9.6	30
45	7.5	3.0	8.0	18

present in the samples examined in this work are subject to the same solvent−solute interactions as the Trp-cage peptide. Table 6 compares experimental values for the cross-relaxation rates of TSP with components of the solvent to values calculated assuming that the experimental values are the result of random encounter of solute and solvent components. Similar to what was observed with Trp-cage, σ_{HF}^{NOE} is larger than predicted while σ_{HH}^{NOE} arising from interaction with water are smaller than expected at all temperatures. These results are consistent with TSP also being preferentially solvated by HFIP to the extent that water molecules are excluded from the region near the surface of the molecule.

DISCUSSION

Hexafluoro-2-propanol is miscible with water in all proportions. However, X-ray diffraction and other techniques show that clusters of fluoro alcohol molecules form in these mixtures, with the extent of cluster formation being maximum at about 30% (v/v) HFIP (*11*, *34*, *53*). At 30% (v/v), the clusters have an apparent Stokes radius of 2.4 nm and consist of both water and HFIP molecules (*53*). It has been argued that formation of clusters in fluoro alcohol−water mixtures is an important aspect of the effects of these mixtures on protein and peptide conformations (*34*). However, this view has been challenged (*11*). It is clear that HFIP and other fluorinated alcohols can associate strongly with proteins (*11*, *12*) although the presence of proteins appears to have little influence on the aggregation behavior of the fluoro alcohol (*11*).

The heterogeneity of the 30% HFIP−water mixture presents some concerns for interpretation of our NOE data. The data obtained from the NMR experiments relate to the bulk or collective behavior of the spins in the sample. If the interchanges between all states involving HFIP are rapid, the measured diffusion coefficients for HFIP would represent the weighted average diffusive behavior of all HFIP molecules: those present in aggregates, those bound to Trp-cage, or those that are monomeric. The diffusion of HFIP in aggregates or bound to the peptide would be slower than diffusion of the monomeric alcohol. It is not possible to access the contributions of each HFIP form to the observed diffusion coefficient in the absence of information about the amounts of HFIP in aggregated states or bound to the peptide. However, we note that the experimental diffusion coefficients for HFIP and the other components of the samples examined are predicted fairly well by hydrodynamic theory that assumes the presence of monomeric alcohol molecules that can be represented by a sphere of reasonable radius. Fortunately, the conclusions of this paper are not sensitive to the exact values of the diffusion coefficients of the peptide or solvent components. No plausible adjustment of the parameters used in the calculations of intermolecular cross-relaxation rates for random interactions of peptide and solvent molecules can produce predictions that are similar to the experimental results at any temperature.

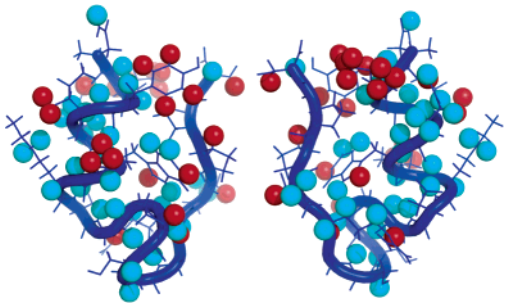

FIGURE 5: A representation of the Trp-cage peptide showing as spheres the hydrogens that experience detected long-lived interactions with HFIP molecules in 30% HFIP−50 mM phosphate buffer at 5 °C. At 45 °C the lifetimes of the peptide−HFIP interactions near the hydrogens indicated by the red spheres become short enough that the interactions with fluoro alcohol molecules at these atoms can be described as diffusive encounters, although the continued presence of long-lived interactions are consistent with the data for many of these spins.

The much larger than expected values of σ_{HF}^{NOE} found for some HFIP−side chain proton interactions at 45 °C suggest that it is likely that the peptide molecule is largely solvated by aggregates of HFIP within which the local molar concentration of fluoro alcohol exceeds the nominal concentration of the bulk sample. Within the peptide-aggregated HFIP complex at 45 °C, the positive σ_{HF}^{NOE} can be interpreted in terms of interactions of HFIP with the peptide hydrogens that appear to be largely diffusive encounters. Provided that the Einstein−Smoluchowski equation applies, it can be estimated that the lifetime of a solvent−peptide encounter under these conditions is of the order of 0.03 ns (*3*, *54*). The observed σ_{HF}^{NOE} could also be due to longer lived encounters. At lower temperatures, the peptide is presumably still solvated by aggregated HFIP, but now the dynamics of the interactions between HFIP and the peptide become increasingly sticky, such that at 5 °C HFIP−side chain encounters have a lifetime of the order of 1 ns, leading to a negative σ_{HF}^{NOE}. The lifetimes of HFIP−peptide encounters may depend on the properties of the HFIP aggregate the peptide is found in, and the effects observed may arise from an average over the multiple types of interactions.

Figure 5 shows the hydrogens of Trp-cage for which experimental σ_{HF}^{NOE} values indicate that long-lived peptide−solvent complexes form in the vicinity of the depicted hydrogen. Most of these atoms are on the surface of the peptide where direct interaction through van der Waals contact with fluoro alcohol molecules is possible. The figure also indicates those side chains where interactions with HFIP appear to become primarily diffusive in nature when the sample temperature is raised.

Molecular dynamics simulations of fluoro alcohol−water and peptide−fluoro alcohol−water systems produce results that are generally in accord with experimental observations, particularly with regard to the selective interaction of fluoro alcohol molecules with peptides in mixed solvents (*55*−*58*). We are not aware of any dynamics trajectories for such systems that have been analyzed with differences in the lifetimes of fluoro alcohol−peptide interactions in mind. It will be of interest to know the extent to which current force

fields and simulation techniques can reproduce observations such as those we report here.

CONCLUSIONS

Our observations of σ_{HF}^{NOE} indicate that the energetics of peptide proton−fluoro alcohol interactions cannot be the same for all hydrogens of the peptide. Some side chain−solvent interactions (e.g., those of Leu2, Tyr3, Ile4, Trp6, and Pro19) may enter the diffusive encounter regime at 45 °C, while fluoro alcohol interactions with other protons, particularly those of the backbone atoms (e.g., HN of Leu2, Trp6, Leu7, and Gly15 and Hα of Ser14 and Arg16), appear to remain essentially intramolecular interactions, with lifetimes of the order of 1 ns at all temperatures studied. Noting the higher temperature sensitivity of the side chain interactions, it must be the case that ΔG for formation of complexes with HFIP near the spins involved is more negative than the values that characterize formation of fluoro alcohol complexes near the backbone hydrogens. Interactions of peptide and proteins with fluoro alcohols presumably involve both hydrophobic effects and hydrogen bonding (*10*), and it is possibly the greater surface exposure of the side chains that leads to stronger interactions with HFIP in their vicinity.

Protein molecules provide rather specific sites with variable affinity for binding organic solvent molecules (*59*−*63*). Presumably, the dynamics of small molecule interactions at these sites vary as well. Our work indicates that even small peptides can selectively interact with organic solvent molecules and demonstrates that different binding sites are characterized by different dynamics of interaction.

ACKNOWLEDGMENT

We thank Professor T. Yamaguchi of Fukuoka University (Japan) for providing densities of HFIP−water mixtures. We are indebted to the authors of the programs DYANA, SPARKY, MOLMOL, and PYmol for making their software available and to Professor K. Plaxco and Dr. B. Baker for facilitating access to the CD instrumentation.

SUPPORTING INFORMATION AVAILABLE

A listing of the proton chemical shifts for Trp-cage at all temperatures examined, indications of the nature and distribution of the intramolecular proton−proton NOEs observed in the structural studies, a plot comparing Cα−H chemical shifts observed to random coil values at 5 °C and upfield spectral data at 25 °C. This material is available free of charge via the Internet at http://pubs.acs.org.

REFERENCES

1. Bagno, A., Rastrelli, F., and Saielli, G. (2005) NMR techniques for the investigation of solvation phenomena and non-covalent interactions, *Prog. NMR Spectrosc. 47*, 41−93.
2. Brand, T., Cabrita, E. J., and Berger, S. (2005) Intermolecular interaction as investigated by NOE and diffusion studies, *Prog. NMR Spectrosc. 46*, 159−196.
3. Otting, G. (1997) NMR studies of water bound to biological molecules, *Prog. NMR Spectrosc. 31*, 259−285.
4. Halle, B. (2004) Protein hydration dynamics in solution: a critical survey, *Philos. Trans. R. Soc. London, Ser. B 359*, 1207−1224.
5. Sundd, M., Kundu, S., and Jagannadham, M. V. (2000) Alcohol-induced conformational transitions in ervatamin C. An alpha-helix to beta-sheet switchover, *J. Protein Chem. 19*, 169−176.
6. Perham, M., Liao, J., and Wittung-Stafshede, P. (2006) Differential effects of alcohols on conformational switchovers in α-helical and β-sheet protein models, *Biochemistry 45*, 7740−7749.
7. Tomaselli, S., Esposito, V., Vangone, P., van Nuland, N. A., Bonvin, A. M. J. J., Guerrini, R., Tancredi, T., Temussi, P. A., and Picone, D. (2006) The α-to-β conformational transition of Alzheimer's Aβ-(1-42) peptide in aqueous media is reversible: A step by step conformational analysis suggest the location of β conformation seeding, *ChemBioChem. 7*, 257−267.
8. Dobson, C. M. (2003) Protein folding and misfolding, *Nature 426*, 884−890.
9. Alexandrescu, A. T. (2005) Amyloid accomplices and enforcers, *Protein Sci. 14*, 1−12.
10. Buck, M. (1998) Trifluoroethanol and colleagues: cosolvents come of age. Recent studies with peptides and proteins, *Q. Rev. Biophys. 31*, 297−355.
11. Gast, K., Siemer, A., Zirwer, D., and Damaschun, G. (2001) Fluoroalcohol-induced structural changes in proteins: some aspects of cosolvent-protein interactions, *Eur. Biophys. J. 30*, 273−283.
12. Kumar, S., Modig, K., and Halle, B. (2003) Trifluoroethanol-induced β → α transition in β-lactoglobulin: Hydration and cosolvent binding by ^{2}H, ^{17}O and ^{19}F magnetic relaxation dispersion, *Biochemistry 42*, 13708−13716.
13. Gerig, J. T. (2004) Structure and solvation of melittin in 1,1,1,3,3,3-hexafluoro-2-propanol/water, *Biophys. J. 86*, 3166−3175.
14. Neidigh, J. W., Fersinmeyer, R. M., and Anderson, N. H. (2002) Designing a 20-residue protein, *Nat. Struct. Biol. 9*, 425−430.
15. Qiu, L., Pabit, S. A., Roitberg, A. E., and Hagen, S. J. (2002) Smaller and faster: The 20-residue Trp-cage protein folds in 4 μs, *J. Am. Chem. Soc. 124*, 12952−12953.
16. Snow, C. D., Zagrovic, B., and Pande, V. S. (2002) The Trp-cage: Folding kinetics and unfolded state topology *via* molecular dynamics simulations, *J. Am. Chem. Soc. 124*, 14548−14549.
17. Kundu, A., and Kishore, N. (2004) Apprent molar heat capacities and apparent molar volumes of aqueous 1,1,1,3,3,3-hexafluoroisopropanol at different temperatures, *J. Solution Chem. 33*, 1085−1095.
18. Palepu, R., and Clarke, J. (1989) Viscosities and densities of 2,2,2-trifluoroethanol + water at various temperatures, *Thermochim. Acta 156*, 359−363.
19. Wu, D., Chen, A., and Johnson, J. C. S. (1995) Improved diffusion-ordered spectroscopy experiment incorporating bipolar-gradient pulses, *J. Magn. Reson. A 115*, 260−264.
20. Zhang, X., Li, C.-G., Ye, C.-H., and Liu, M.-L. (2001) Determination of molecular self-diffusion coefficients using multiple spin-echo NMR spectroscopy with removal of convection and background gradient artifacts, *Anal. Chem. 73*, 3528−3534.
21. Jerschow, A., and Muller, N. (1997) Suppression of convection artifacts in stimulated-echo diffusion experiments. Double-stimulated-echo experiments, *J. Magn. Reson. 125*, 372−375.
22. Fulton, D. B., and Ni, F. (1997) ROESY with water flip back for high field NMR of biomolecules, *J. Magn. Reson. 129*, 93−97.
23. Gerig, J. T. (2005) Selective solvation in a fluorous reaction system, *J. Am. Chem. Soc. 127*, 9277−9284.
24. Gerig, J. T. (2003) Solute-solvent interactions probed by intermolecular NOEs, *J. Org. Chem. 68*, 5244−5248.
25. Koradi, R., Billeter, M., and Wuthrich, K. (1996) MOLMOL: A program for display and analysis of molecular structures, *J. Mol. Graphics 14*, 51−55.
26. Connolly, M. L. (1983) Analytical molecular surface calculation, *J. Appl. Crystallogr. 16*, 548−558.
27. Gordon, A. J., and Ford, R. A. (1972) *The Chemist's Companion*, Wiley-Interscience, New York.
28. Gerig, J. T., and Strickler, M. A. (2002) Intermolecular Overhauser effects in fluoroalcohol solutions of *cyclo*-alanylglycine, *Biopolymers 64*, 227−235.
29. Otting, G., Liepinsh, E., Halle, B., and Frey, U. (1997) NMR identification of hydrophobic cavities with low water occupancies in protein structures using small gas molecules, *Nat. Struct. Biol. 5*, 396−404.
30. Goddard, T. D., and Kneller, D. G. SPARKY3, University of California, San Francisco.
31. Guntert, P., Mumenthaler, C., and Wuthrich, K. (1997) Torsional angle dynamics for NMR structure calculation with the new program DYANA, *J. Mol. Biol. 273*, 283−298.
32. Güntert, P. (2004) Automated NMR protein structure calculation with CYANA, *Methods Mol. Biol. 278*, 353−378.

33. Case, D. A., and Wright, P. E. (1993) Determination of high-resolution NMR structures of proteins, in *NMR of Proteins* (Clore, G. M., and Gronenborn, A. M., Eds.) pp 53−91, CRC, Boca Raton, FL.
34. Hong, D.-P., Hoshino, M., Kuboi, R., and Goto, Y. (1999) Clustering of fluorine-substituted alcohols as a factor responsible for their marked effects on proteins and peptides, *J. Am. Chem. Soc. 121*, 8427−8433.
35. Barua, B., and Anderson, N. H. (2002) Determinants of miniprotein stability: can anything replace a buried H-bonded Trp sidechain? *Lett. Pept. Sci. 8*, 221−226.
36. Baxter, N. J., and Williamson, M. P. (1997) Temperature dependence of ^{1}H chemical shifts in proteins, *J. Biomol. NMR. 9*, 359−369.
37. Merutka, G., Dyson, H. J., and Wright, P. E. (1995) "Randon coil" ^{1}H chemical shifts obtained as a function of temperature and trifluoroethanol concentration for the peptide series GGXGG, *J. Biomol. NMR 5*, 14−24.
38. Schwarzinger, S., Kroon, G. J. A., Foss, T. R., Chung, J., Wright, P. E., and Dyson, H. J. (2001) Sequence-dependent correction of random coil NMR chemical shifts, *J. Am. Chem. Soc. 123*, 2970−2978.
39. Wishart, D. S., and Sykes, B. D. (1994) Chemical shifts as a tool for structure determination, in *Methods in Enzymology* (James, T. L., and Oppenheimer, N. J., Eds.) pp 363−392, Academic, San Diego, CA.
40. Sreerama, N., and Woody, R. W. (2004) Computation and analysis of protein CD spectra, *Methods Enzymol. 383*, 318−351.
41. Esturau, N., Sanchez-Ferrando, F., Gavin, J. A., Roumestand, C., Delsuc, M.-A., and Parrella, T. (2001) The use of sample rotation for minimizing convection effects in self-diffusion NMR experiments, *J. Magn. Reson. 153*, 48−55.
42. Gierer, A., and Wirtz, K. (1953) Molecular theory of microfriction, *Z. Naturforsch. A: Phys. Sci. 8*, 532−538.
43. Neuhaus, D., and Williamson, M. P. (2000) *The Nuclear Overhauser Effect in Structural and Conformational Analysis*, 2nd ed., Wiley-VCH, New York.
44. Noggle, J. H., and Schirmer, R. E. (1971) *The Nuclear Overhauser Effect*, Academic, New York.
45. Ayant, Y., Belorizky, E., Fries, P., and Rosset, J. (1977) Effet des interactions dipolaires magnetiques intermoleculaires sur la relaxation nucleaire de molecules polyatomiques dans les liquides, *J. Phys. (Paris) 38*, 325−337.
46. Bagno, A., Compulla, M., Pirana, M., Scorrano, G., and Stiz, S. (1999) Preferential solvation of organic species in binary solvent mixtures probed by intermolecular ^{1}H NOESY NMR spectroscopy, *Chem. Eur. J. 5*, 1291−1300.
47. Diaz, M. D., and Berger, S. (2001) Preferential solvation of a tetrapeptide by trifluoroethanol as studied by intermolecular NOE, *Magn. Reson. Chem. 39*, 369−373.
48. Diaz, M. D., Fioroni, M., Burger, K., and Berger, S. (2002) Evidence of complete hydrophobic coating of bombesin by trifluoroethanol in aqueous solution: An NMR spectroscopic and molecular dynamics study, *Chem. Eur. J. 8*, 1663−1669.
49. Halle, B. (2003) Cross-relaxation between macromolecular and solvent spins: The role of long-range dipole couplings, *J. Chem. Phys. 119*, 12372−12385.
50. Frezzato, D., Rastrelli, F., and Bagno, A. (2006) Nuclear spin relaxation driven by intermolecular dipolar interactions: The role of solute-solvent pair correlations in the modeling of spectral density functions, *J. Phys. Chem. B 110*, 5676−5689.
51. Halle, B., and Carlstrom, G. (1981) Hydration of ionic surfactant micelles from water oxygen-17 magnetic relaxation, *J. Phys. Chem. 85*, 2142−2147.
52. Otting, G., and Liepinsh, E. (1995) Protein hydrations viewed by high-resolution NMR spectroscopy: Implications for magnetic resonance image contrast, *Acc. Chem. Res. 28*, 171−177.
53. Yoshida, K., Yamaguchi, T., Adachi, T., Otomo, T., Matsuo, D., Takamuku, T., and Nishi, H. (2003) Structure and dynamics of hexafluoroisopropanol-water mixtures by x-ray diffraction, small angle neutron scattering, NMR spectroscopy and mass spectrometry, *J. Chem. Phys. 119*, 6132−6142.
54. Islam, M. A. (2004) Einstein-Smoluchowski diffusion equation: A discussion, *Phys. Scr. 70*, 120−125.
55. Smith, P. E. (1999) Computer simulation of cosolvent effects on hydrophobic hydration, *J. Phys. Chem. B 103*, 525−534.
56. Dwyer, D. S. (1999) Molecular simulation of the effects of alcohols on peptide structure, *Biopolymers 49*, 635−645.
57. Fioroni, M., Diaz, M. D., Burger, K., and Berger, S. (2002) Solvation phenomena of a tetrapeptide in water/trifluoroethanol and water/ethanol mixtures: A diffusion NMR, intermolecular NOE and molecular dynamics study, *J. Am. Chem. Soc. 124*, 7737−7744.
58. Roccatano, D., Fioroni, M., Zacharias, M., and Colombo, G. (2005) Effect of hexafluoroisopropanol alcohol on the structure of melittin: A molecular dynamics simulation study, *Protein Sci. 14*, 2582−2589.
59. Liepinsh, E., and Otting, G. (1997) Organic solvent identify specific ligand binding sites on protein surfaces, *Nat. Biotechnol. 15*, 264−268.
60. English, A. C., Done, S. H., Caves, L. S. D., Groom, C. R., and Hubbard, R. E. (1999) Locating interaction sites on proteins: The crystal structure of thermolysis soaked in 2% to 100% isopropanol, *Proteins: Struct., Funct., Genet. 37*, 628−640.
61. Mattos, C., and Ringe, D. (2001) Proteins in organic solvents, *Curr. Opin. Struct. Biol. 11*, 761−764.
62. Martinez, D., and Gerig, J. T. (2001) Intermolecular ^{1}H{^{19}F} NOEs in studies of fluoroalcohol-induced conformations of peptides and proteins, *J. Magn. Reson. 152*, 269−275.
63. Mattos, C., Bellamacina, C. R., Peisach, E., Pereira, A., Vitkup, D., Petsko, G. A., and Ringe, D. (2006) Multiple solvent crystal structures: Probing binding sites, plasticity and hydration, *J. Mol. Biol. 357*, 1471−1482.

BI061750+